Joint Torque Sensory Feedback in the Control of a PUMA Manipulator

LAWRENCE E. PFEFFER, STUDENT MEMBER, IEEE, OUSSAMA KHATIB, MEMBER, IEEE, AND JOHN HAKE

Abstract—**Accurate control of joint torques is essential to achieve high performance in advanced assembly and other tasks that involve fine motion, active force control, or high-speed operations. Joint torque control can be substantially improved by sensory feedback. In this paper we present the design and describe the actual characteristics of a joint torque sensor for a PUMA 500. Using this sensor, a joint torque servomechanism has been designed and implemented. A model of the actuator-transmission-load system, including flexibility, was developed and verified using both time- and frequency-domain techniques. Compensators based on this model were designed and tested. Experimental results obtained from pure torque control and joint motion tracking are presented. These results demonstrate a significant reduction of the effective friction (97 percent), and a substantial improvement in fine motion control.**

I. Introduction

TODAY'S industrial robots are almost exclusively position-controlled devices. This type of control has proven to be adequate for some industrial tasks, such as material handling. However, these robots have made few inroads into applications such as precision assembly because of the inevitable variations in real-world assembly tasks. Tolerances in mating parts, fixtures, and grippers all contribute to uncertainty in the relative positions of mating parts. This uncertainty frequently results in large mating forces as well as jamming during assembly. A more promising approach is to control both the forces a manipulator exerts on an object and the motions of the end-effector [6], [11]. Accurate control of joint forces is a key ability for robot manipulators aimed at achieving high performance in motion and active force control.

Most industrial robots use transmission devices which introduce significant disturbance torques at the joints. In revolute joint robots, gear reductions are commonly used as transmission devices, and are typically overmeshed in order to minimize backlash. However, this approach introduces large radial gear forces which increase both the gear cogging and the drive friction. Cogging occurs as each tooth on one gear is wedged between the two mating teeth on the opposing gear. This wedging action introduces a disturbance (ripple) torque whose frequency is proportional to both the pitch of the gears and the joint velocity. This problem is exacerbated by any eccentricities in the pitch lines of the gears.

One method of compensation for these disturbance torques is to sense the transmitted torque at the joint and close a torque servo around the motor and transmission system. Such a design has been implemented [12] for a single-joint manipulator. The system demonstrated a wide bandwidth, and a reduction of 95 percent in the effective friction. The first two joints of a Stanford Arm were redesigned [7] to accommodate torque sensors. This torque feedback reduced the effective friction torque by 97 percent. Joint torque sensing has been recently implemented [2] in a direct-drive manipulator. This sensor design has provided high sensitivity while maintaining high mechanical stiffness.

In this paper we will describe the design and construction [5] of a joint torque sensor for the third joint of a PUMA 500. We will also present the implementation of a control system based on joint torque sensory feedback for fine motion and force control.

II. Joint Torque Sensor Design

The PUMA 500, shown in Fig. 1, is a five-degree-of-freedom revolute joint manipulator. Joint three is driven by a modular encoder-motor-brake package located in the rear of link 2. Torque is delivered to the joint axis through flexible couplings, a drive shaft, and a two-stage gear reduction. The first gear reduction is (see Fig. 2) a bevel gear set, and the second reduction is a spur gear driving a bull or ring gear. In the standard PUMA, the bull gear is bolted to the face of link 3, and transmits the torque directly to link 3.

Ideally, the sensor should measure only the drive torque transmitted at a joint. Unfortunately, this requires the sensor to transmit a complex set of support forces and moments while maintaining good sensitivity solely to the drive torque. In our design, the sensor has been placed between the bull gear (see Fig. 2) and link 3, replacing the standard attachment bolts with flexures instrumented with stain gauges. Although this sensor location does not allow the sensor to account for friction in the joint bearings, it is dictated by the shape of the existing joint castings. During operation, the modified joint can only transmit torque (from the bull gear) to link 3 via the overload ring and three steel support flexures. The strain in the flexures is measured with strain gauges and amplified to

Manuscript received July 14, 1986; revised October 11, 1988. This work was supported by the National Science Foundation under Contract MEA80-19628, a grant from the Systems Development Foundation, and DARPA under Contract MDA 903-86-K-0037. Part of the material, in this paper was presented at the American Control Conference, Seattle, WA, June 18-20, 1986.

L. Pfeffer is with the Aerospace Robotics Laboratory, Department of Aeronautics and Astronautics, Stanford University, Sanford, CA 94305.

O. Khatib is with the Robotics Laboratory, Computer Science Department, Stanford University, Stanford, CA 94305.

J. Hake was with the Design Division, Mechanical Engineering Department, Stanford University, Stanford, CA 94305. He is now with Adept Technology Inc., San Jose, CA 95134.

IEEE Log Number 8927075.

1042-296X/89/0800-0418$01.00

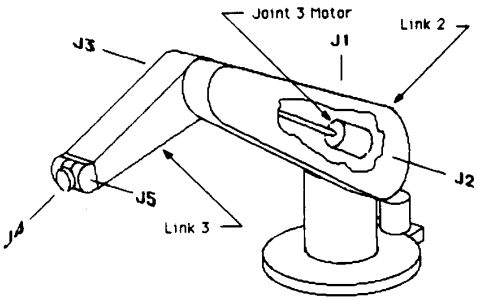

Fig. 1. PUMA 500 robot manipulator.

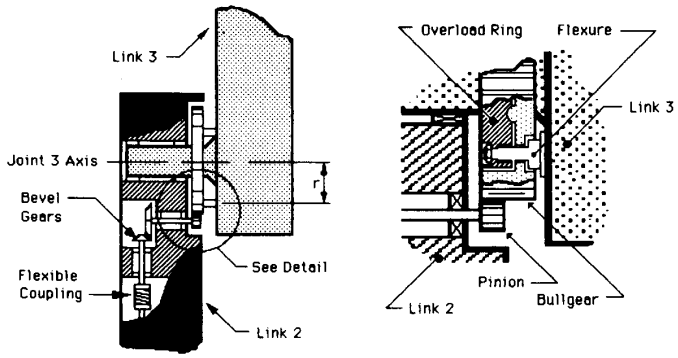

Fig. 2. Detailed of instrumented joint.

provide an analog voltage proportional to the transmitted torque.

The force transmitted by the gear to each flexure can be resolved into three components: a force tangent to the pitch circle of the bull gear, a force which is radial with respect to the pitch circle, and a force that is parallel to the joint axis. Of these three, only the forces tangent to the pitch circle transmit torque. The joint torque γ_3 transmitted through the three support flexures is

$$\gamma_3 = \sum_{i=1}^{3} (rp_i) \tag{1}$$

where r is the radial distance of the each flexure to the joint axis, and p_i is the tangent force of the gear on the ith flexure (see Fig. 2). The average tangent force $\bar{p}$ of the gear is

$$\bar{p} = \frac{\gamma_3}{3r}. \tag{2}$$

The support flexures are bolted to the overload ring at one end, and to the link at the other. Each flexure reacts to the gear forces as a beam in bending, fixed on one end, and guided on the other (Fig. 3). This beam is statically indeterminate with respect to moments. To solve for the bending moment, the shear $v(x)$ is written as a function of the distance x along the flexure, the tangential deflection y, and the beam properties E (the Young's modulus of the material) and I (the area moment of inertia for the beam cross section) [10].

$$v(x) = \frac{d}{dx}\left(EI\frac{d^2y}{dx^2}\right). \tag{3}$$

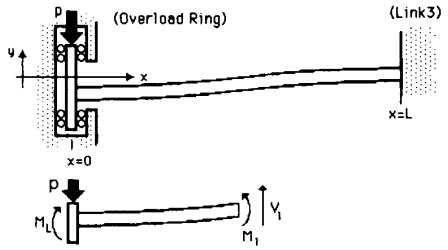

Fig. 3. Beam model.

This equation can be integrated once to find the bending moment, twice to find the slope, and a third time to find deflection. The constants of integration are found from the boundary conditions, i.e., zero deflection and slope at the link 3 surface, and zero slope at the overload ring. This yields the bending moments $M(x)$

$$M(x) = \frac{p(2x-L)}{2} \tag{4}$$

for x varying from zero to L, its full length (see Fig. 3). For practical reasons (attachments, geometrical constraints), the cross section of the beam cannot be uniform. The beam has been designed to have six distinct cross sections, as shown in Fig. 4. The sections (left to right) are: threads for installation in the overload ring, a shoulder for centering the flexure in the overload ring, the active (gauge) section, the overload shoulder, the (wrench) shoulder for use during installation, and the threaded section for installation in link 3. We have designed the flexure so that the greatest strains occur only in the relatively thin section where the strain gauges are placed.

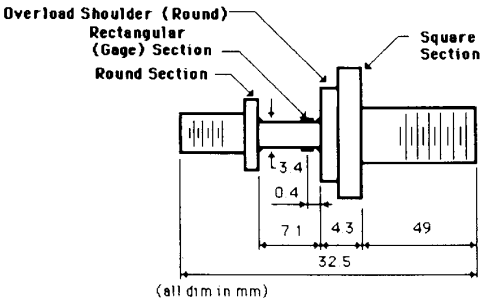

Fig. 4. Flexure.

A general model for this beam bas been developed using the previous analysis. The boundary conditions of bending moment, slope, and deflection are set equal at each section change. The bending moment at the base of the active beam section is

$$M(x)=\frac{p(2x-\lambda)}{2} \tag{5}$$

where λ is a boundary condition matching constant related to the lengths and area moments of the beam sections that comprise the flexure [5]. The bending stress $\sigma(x)$ is [10]

$$\sigma(x)=\frac{CK_tM(x)}{I} \tag{6}$$

where C is the half thickness of the beam, and K_t is the stress concentration factor for the section change. The strain is related to the stress by Hooke's law [10]

$$\epsilon(x)=\frac{\sigma(x)}{E}. \tag{7}$$

Substituting (6) into (7) yields

$$\epsilon(x)=\frac{CK_tM(x)}{IE}. \tag{8}$$

The relationship between strain and joint torque is found using (2), (5), and (8)

$$\frac{\epsilon(x)}{\gamma_3}=\frac{CK_t\left(x-\frac{\lambda}{2}\right)}{3rIE}. \tag{9}$$

We iterated through several different designs before finding the best compromise of sensitivity and stiffness. The final dimensions of the beam are shown in Fig. 4. With the mechanical parameters in Table I, the strain per joint torque scale factor is

$$\frac{\epsilon}{\gamma_3}=14.25\mu\epsilon/\text{N}\cdot\text{m}. \tag{10}$$

To sense the strain in the flexures, each is fitted with four 350-Ω copper–constantan foil gauges, with two gauges on each of the indicated flexure surfaces that are normal to the tangent direction of the bull gear. The four gauges on each flexure are arranged in a full Wheatstone bridge configuration [8], [9].

TABLE I
MECHANICAL PARAMETERS

$x = 4.7 \times 10^{-3}$ m	gauge position
$\lambda = 1.63 \times 10^{-2}$ m	beam section constant
$K_t = 1.88$	stress concentration factor
$C = 1.65 \times 10^{-3}$ m	beam half thickness
$r = 5.02 \times 10^{-2}$ m	flexure to joint axis distance
$I = 2.38 \times 10^{-11}$ m^4	area moment of inertia at gauge
$E = 2.07 \times 10^{11}$ Pa	Young's modulus for steel

The sensor geometry and the full Wheatstone bridge makes the sensor flexures sensitive to the joint torque, yet relatively insensitive to radial or axial forces. Using a gauge factor of 2.05 (for copper–constantan) and a 5.0 V dc input excitation (limited primarily by thermal considerations), the bending strains due to tangential gear forces reduced to

$$\frac{V_{\text{out}}}{\epsilon}=gV_{\text{in}}=10.25\ \mu\text{V}/\mu\epsilon. \tag{11}$$

The gain of each bridge output voltage per joint torque is therefore

$$\frac{V_{\text{out}}}{\gamma_3}=146\ \mu\text{V/N}\cdot\text{m}. \tag{12}$$

Each of the three support flexures has been instrumented (gauged) identically. Each has its bridge signal individually buffered, amplified by a factor of 1000, and then the three signals are summed (each with a weight of unity). The overall scale factor is thus 3000 times the raw bridge signal for a single one of the three flexures

$$\frac{V_{\text{sensor}}}{\gamma_3}=\frac{3000V_{\text{out}}}{\gamma_3}=438\ \text{mV/N}\cdot\text{m}. \tag{13}$$

The stress in each flexure due to the maximum motor torque, 90 N·m [1], is computed using (2), (5), and (6), and equal to 2.68×10^8 Pa, a factor of safety of 2.3 for 4140 steel.

To prevent damage during a crash, the sensor has an overload protection feature. The force transmitted to the sensor is limited to less than four times the peak static load. The bull gear is clamped (see Fig. 5) to the overload ring by springs, and three cones on the face of the overload ring seat into recesses in the face of the gear. As the gear forces exceed the desired limit, the cones unseat, and the gear rotates slightly to drive directly against the base of the flexures. As the gear forces subside, the cones reseat and the gear moves back to its normal position. This mechanism limits the forces exerted on the instrumented portion of the flexure to the breakaway force set by the springs.

Experimental Sensor Characteristics

The sensitivity of the sensor has been measured as 159 mV/N·m. This is 36 percent of the gain predicted by (13). The difference is due to the strain gauges averaging over an area substantially larger than the stress concentration. There is a

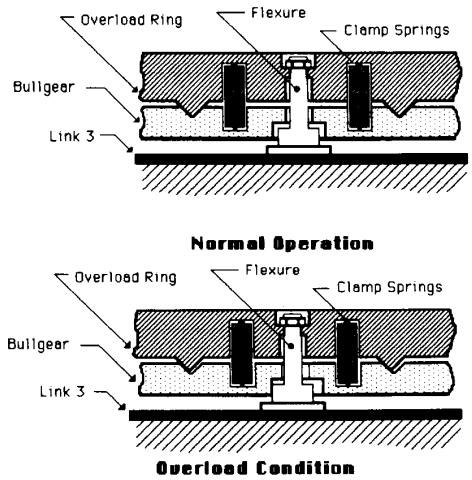

Fig. 5. Overload protection.

slight hysteresis, approximately 28 mV, which corresponds to 0.18 N·m. Sensitivity should be constant, regardless of the joint 3 position. To evaluate the position dependency of the sensor, joints 2 and 3 were rotated in 10° increments to modify the position of joint 3 while keeping link 3 horizontal. The output of the sensor varied by 8 percent over 270°. This variation is nonlinear. This is expected to be the result of the complex loading produced as the pinion rolls over the portions of the gear adjacent to the flexures.

III. Joint Torque Control

In this section, a model of the actuator-transmission-load system of the instrumented third joint is developed and experimentally verified using both time- and frequency-domain techniques. A schematic of the actuator-transmission-load system is shown in Fig. 6. This includes the motor, the driveshaft, the gear reduction, the sensor, and the link. θ_m and θ_3 represent the angular coordinates of the motor shaft and the third link, respectively. γ_m and γ_3 are the torques at the motor and the link. The definition and values of the various parameters of the system are given in Table II.

The motor is driven by an amplifier with current feedback, with a bandwidth much higher than the rest of the system. This dc motor exhibits considerable brush friction. An optical encoder, for measurement of motor shaft angle, introduces negligible inertia and friction. The driveshaft on this early PUMA is hollow and connected at each end by couplings; the main effect is torsional flexibility. Two stages of gear reduction couple the motor torque to the load. The cogging friction and backlash from the gearing appeared significantly smaller than the motor friction effects, backlash was neglected, and the average friction contribution due to the gears was combined with the motor friction. The sensor adds both flexibility and hysteresis to the system, but, by design, of such small amounts that they can be neglected. The link is modeled as a rigid body, whose inertia includes any outboard payloads (the rigidity of the link structure is an area for future investigation).

Linear damping, primarily due to viscous effects in bearings, was estimated and included in the model

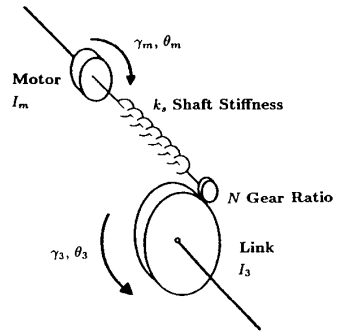

Fig. 6. Actuator-transmission-load system.

TABLE II
ACTUATOR - TRANSMISSION SYSTEM PARAMETERS

$g_a = 5.0 \times 10^{-1}$ A/V	amplifier gain
$g_s = 1.59 \times 10^{-1}$ V/N·m	torque sensor gain
$k_m = 2.793 \times 10^{-1}$ N·m/A	motor torque constant
$I_m = 2.88 \times 10^{-4}$ kg·m^2	motor inertia
$I_3 = 3.36 \times 10^{-1}$ kg·m^2	inertia of link 3
$N = 53.37063$	gear ratio
$k_s = 5.57$ N·m/rad	shaft torsional stiffness
$f_3 = 14.7$ N·m·s	joint 3 linear friction

$$I_m\ddot{\theta}_m + f_c(\theta_m, \dot{\theta}_m) + f_m\dot{\theta}_m + k_s(\theta_m - N\theta_3) = \gamma_m \tag{14}$$

$$I_3\ddot{\theta}_3 + f_3\dot{\theta}_3 + Nk_s(N\theta_3 - \theta_m) = 0 \tag{15}$$

$$-Nk_s(N\theta_3 - \theta_m) = \gamma_3. \tag{16}$$

$f_c(\theta_m, \dot{\theta}_m)$ is the nonlinear friction, and the motor torque is

$$\gamma_m = k_m g_a U \tag{17}$$

where U is the amplifier voltage command. The joint torque sensor voltage output is

$$V_s = g_s\gamma_3. \tag{18}$$

The motor torque constant was found from manufacturer's data, and verified. The parameters I_m, I_3, and N were obtained from [1]. k_s and f_3 have been estimated from the time response of the link when the motor is locked, using (15). Ignoring the motor friction, the transfer function of motor torque to joint torque is given by

$$\frac{\Gamma_3(s)}{\Gamma_m(s)} = \frac{\dfrac{Nk_s}{I_m}\left(s + \dfrac{f_3}{I_3}\right)}{\left(s^3 + \dfrac{f_3}{I_3}s^2 + \dfrac{(N^2I_m + I_3)k_s}{I_mI_3}s + \dfrac{f_3k_s}{I_mI_3}\right)}. \tag{19}$$

The use of the numerical values of Table I in this transfer function yields a real zero at 43.75 rad/s (6.96 Hz), a real pole at 12.79 rad/s (2.04 Hz), and a pair of complex poles corresponding to a natural frequency of 257.22 rad/s (40.9 Hz) with a damping factor of 0.06.

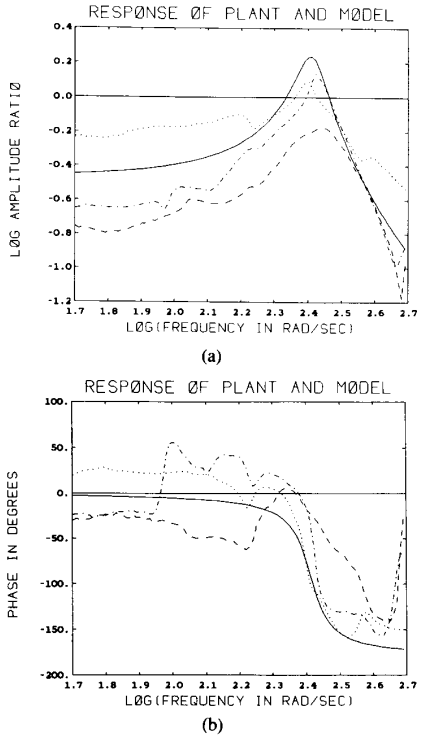

Fig. 7. (a) Amplitude response. (b) Phase response.

The experimental frequency responses conducted at various driving amplitudes have shown close agreement with the complex pole pair near and beyond the resonant frequency (see Fig. 7). At low frequencies, 10 Hz and below, experimental data had a fairly flat response. In this regime in fact, the nonlinear friction is dominant and the effect of real pole and zero are masked. This behavior at low frequencies suggests a reduction of the transfer function to the system's second-order dominant behavior [3]. The simplified transfer function is

$$\frac{\Gamma_3(s)}{\Gamma_m(s)} = \frac{\dfrac{Nk_s}{I_m}}{s^2 + 2\xi\omega s + \omega^2}. \tag{20}$$

ξ and ω have been estimated to be 0.1 and 259.3 rad/s from a series of experimental measurements. These values closely correspond to those obtained above.

When the link is immobilized, the transfer function can be found by considering the limit as the link inertia becomes infinite. This yields

$$\left[\frac{\Gamma_3(s)}{\Gamma_m(s)}\right]_c = \frac{\dfrac{Nk_s}{I_m}}{s^2 + 2\xi\omega_c s + \omega_c^2} \tag{21}$$

where $\omega_c = \sqrt{(k_s/I_m)} = 139.1$ rad/s.

Since the nonlinear friction is neglected in these transfer functions, the simplified model must be compared to the actual behavior of the system during motion. We made measurements of sinusoidal input describing functions over the range of frequencies and amplitudes of concern. Fig. 7(a) and (b) compares the actual amplitude and phase characteristics of the plant for three different levels of excitation to those of the simplified model. These experimental measurements show the simplified model to be a reasonable basis for control design. This model has, in fact, a greater amplitude at the resonance than the plant. It also exhibits more phase lag at and above the resonance.

IV. Digital Compensator Design

The continuous transfer functions were discretized using the zero-order hold technique with a sample period of 0.002 s. The discrete transfer functions for the free and constrained case are

$$\frac{V_s(z)}{U(z)} = \frac{0.04329549z + 0.041819}{z^2 - 1.6546z + 0.90196}$$

$$\left[\frac{V_s(z)}{U(z)}\right]_c = \frac{0.045123z + 0.044292}{z^2 - 1.8711z + 0.94588}. \tag{22}$$

Experiments with first-order compensators have shown insufficient performance. This limitation is due to the flexibility in the transmission and the separation of the sensor from the actuator. Second-order compensators for the free and constrained cases, placed in the torque feedback path, were designed using Z-plane root loci [4]

$$H(z) = k\,\frac{0.9268z^2 - 1.4829z + 0.6511}{z^2 - 0.95z + 0.046}$$

$$H_c(z) = k_c\,\frac{1.9z^2 - 2.28z + 0.76}{z^2 - 0.65z + 0.03} \tag{23}$$

where the dc gains k and k_c were both set equal to 5.0. The performance was limited both by power amplifier saturation and by computation and sampling delays. The Z-plane root locus accounts for the effective half sample delay (roughly 14° near resonance), but not for the added computational delay. The computation delay from reading sensors to sending commands was measured and found to be 0.4 ms. This delay corresponds to roughly six degrees of phase shift at a frequency of 40 Hz (roughly, the free-arm resonant frequency) and is smaller than the sampling delay. Faster sampling and computation would lead to a better system, with greater damping and phase margins, but were not achievable with the hardware and software available. The Z-plane root loci are shown in Fig. 8.

First, pure torque control experiments have been conducted. Without compensation, the open-loop system shows no response to the square-wave torque input of amplitude less than 1.5 N·m, as shown in Fig. 9(a).

Fig. 9(b) shows the response of the closed-loop system resulting in an overshoot and a steady-state error of 30 and 7 percent, respectively. Compared to the open-loop response performance, this represents a 97-percent reduction in the effective friction. The 10–90-percent rise time is less than 0.01 s (only five sample periods), as shown in Fig. 9(c), where

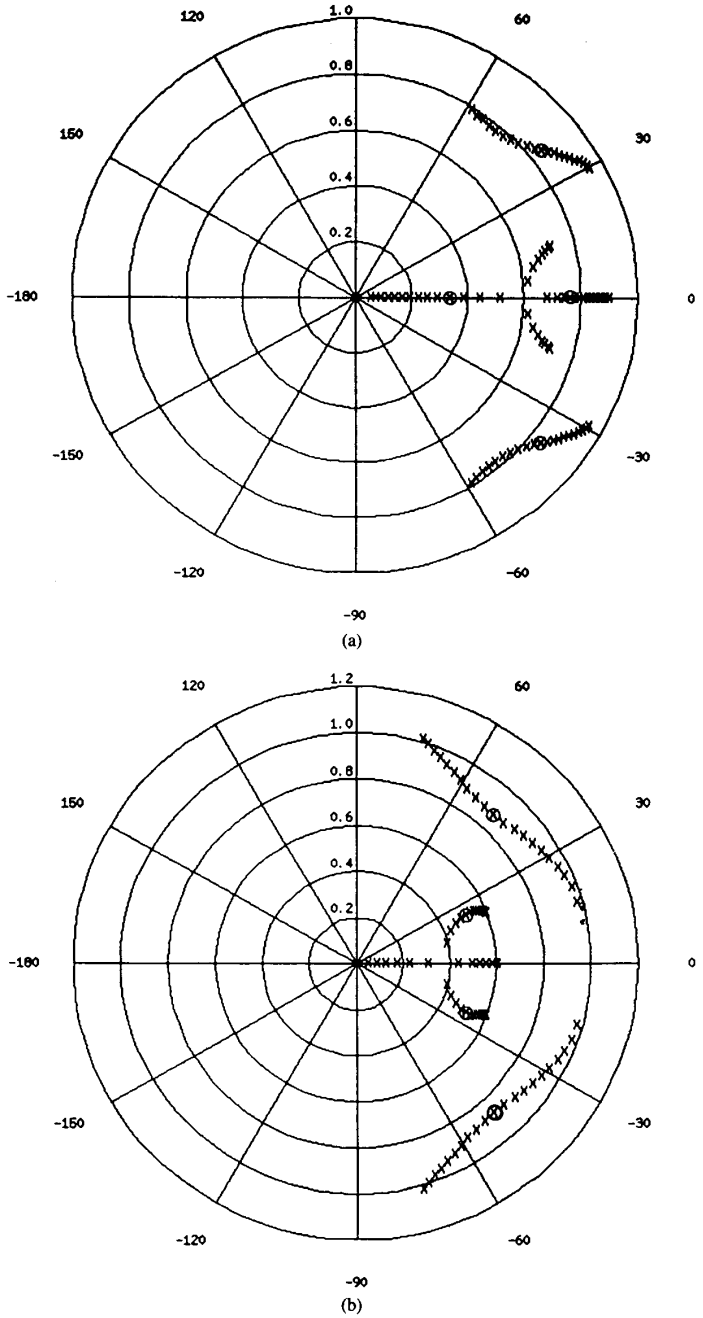

Fig. 8. (a) *Z*-plane root locus: Free motion case. (b) *Z*-plane root locus: Constrained motion case.

the time scale has been expanded. Considering the open-loop resonant period (0.045 s), this represents a substantial increase in bandwidth.

For joint position tracking, the joint torque feedback compensator is an inner loop in a joint position feedback servo. A simple lead/lag compensator has been selected for the outer position servo. Fig. 10(a) shows the position response to sinusoidal input (1 Hz, 0.1 rad), without joint torque compensation. At this level of amplitude, very poor and nonrepeatable performance can be observed. The response when the joint torque compensator is included is shown in Fig. 10(b). The tracking error is approximately 14 percent.

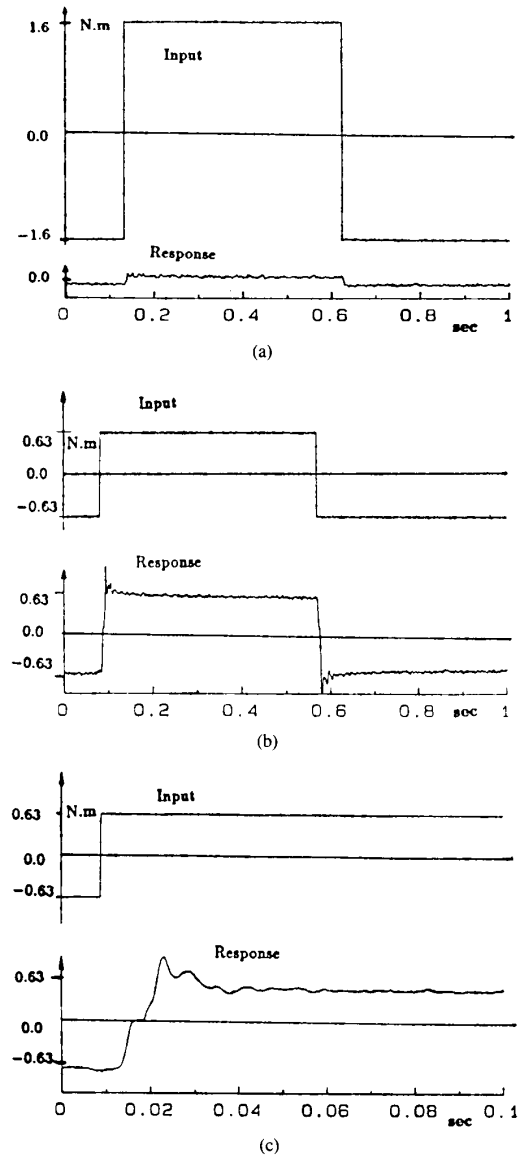

Fig. 9. (a) Torque open-loop response. (b) Torque closed-loop response. (c) Torque closed-loop response: Expanded time scale.

V. Conclusion

A joint torque sensor for the third joint of a PUMA 500 manipulator has been designed and constructed. This sensor exhibits a sensitivity of 159 mV/N·m with an acceptable level of nonlinearity (8 percent), and provides overload protection. A simplified dynamic model of the actuator–transmission–load system, including flexibility and linear friction has been developed. Accurate modeling of the flexibility was essential for the control design due to the separation of the sensor from the actuator. Compared with the system's actual response, this model has been shown to be a good basis for control design. Digital compensators for pure torque control and unconstrained joint motion were designed and tested. These compensators demonstrated a significant improvement in fine motion

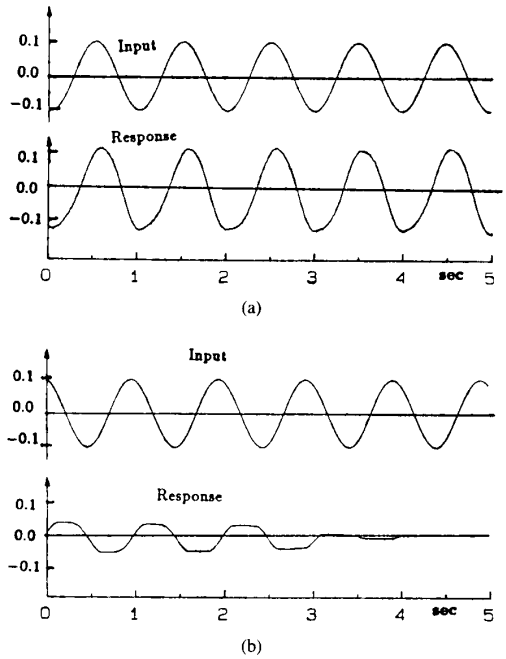

Fig. 10 (a) Open-loop tracking. (b) Closed-loop tracking.

control providing a substantial reduction of the effective friction (97 percent).

The overall stability and performance of the system are dependent on the sensor characteristics, the flexibility, and nonlinearity of the mechanism. As indicated by the model, the effects of motor inertia and friction are magnified by the high gearing ratio of this manipulator. Direct- or semi-direct-drive mechanisms are, therefore, attractive approaches to reduce these effects, assuming they provide similar efficiencies in actuation. Improved modeling, nonlinear friction compensation, and analog implementation of the joint torque feedback loop can be expected to further enhance the level of performance that has been demonstrated here.

Acknowledgment

The authors would like to thank B. Carlisle, D. Allan (both from Unimation West, now Adept Technology Inc.), and Prof. B. Roth for their support and technical assistance in the design and construction of the joint sensor. They would also like to thank B. Armstrong, S. Shekhar, and D. Vischer for help in the preparation of the manuscript.

References

[1] B. Armstrong, O. Khatib, and J. Burdick, "The explicit dynamic model and inertial parameters of the PUMA 560 arm," in *Proc. 1986 IEEE Conf. on Robotics and Automation*, pp. 510–518, Apr. 1986.

[2] H. Asada, K. Youcef-Toumi, and S. K. Lim, "Joint torque measurement of a direct-drive arm," in *Proc. 23rd IEEE Conf. on Decision and Control*, pp. 1332–1337, Dec. 1984.

[3] R. H. Cannon, *Dynamics of Physical Systems*. New York, NY: McGraw-Hill, 1967, pp. 251.

[4] G. F. Franklin and J. D. Powell, *Digital Control of Dynamic Systems*. Reading, MA: Addision-Wesley, 1980.

[5] J. C. Hake and J. Farah, "Design of a joint torque sensor for the

unimation PUMA 500 robot arm," Final Rep., ME 210, Stanford Univ., Stanford, CA, 1984.
[6] O. Khatib, "The operational space formulation in the analysis, design, and control of manipulators," in *Robotics Research: The Third International Symposium*, O. Faugeras and G. Giralt, Eds. Cambridge, MA: MIT Press, 1986, pp. 261-270.
[7] J. Y. S. Luh, W. B. Fisher, and R. P. Paul, "Joint torque control by direct feedback for industrial robots," *IEEE Trans. Automat. Contr.*, vol. AC-28, no. 2, Feb. 1983.
[8] H. N. Norton, *Sensor and Analyzer Handbook*. Englewood Cliffs, NJ: Prentice-Hall, 1982, pp. 145-155.
[9] R. E. Peterson, *Stress Concentration Factors*. New York, NY: 1974.
[10] E. P. Popov, *Mechanics of Materials* (SI Version), 2nd ed. Englewood Cliffs, NJ: Prentice-Hall, 1978.
[11] M. Raibert and J. J. Craig, "Hybrid position force control of manipulators," *ASME J. Dynamic Syst., Meas., Contr.*, June 1981.
[12] C. H. Wu and R. P. Paul, "Manipulator compliance based on joint torque control," in *Proc. 19th IEEE Conf. on Decision on Control*, vol. 1, pp. 84-88, Dec. 1980.

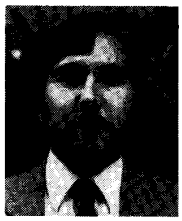

Lawrence E. Pfeffer (S'86) received the degree in applied science from the University of California, San Diego, in 1980, and the M.S. degree in aeronautics and astronautics from Stanford University, Stanford, CA, in 1984.

His professional interests have been variously, high-energy physics, communication/computer systems, dynamics/control, and robotics. Currently he is a Ph.D. candidate at Stanford University, pursuing research at Stanford's Aerospace Robotics Laboratory in the area of cooperative control of robot manipulators.

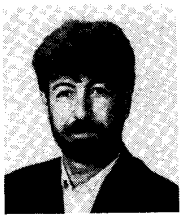

Oussama Khatib (M'85) received the degree of "Docteur-Ingénieur en Automatique et Système" in 1980 from "l'École Nationale Supérieure de l'Espace," Toulouse, France.

He is a Senior Research Associate leading the *Manipulation Project* at the Robotics Laboratory, Computer Science Department, Stanford University, Stanford, CA. His research interests, include motion and force control, motion primitives and sensor-based strategies for real-time collision avoidance and part mating operations, and design of high-performance force-controlled manipulator and micro-manipulator systems.

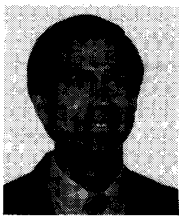

John Hake received the B.S. degree in mechanical engineering from the University of Illinois, Urbana, in 1982, and the M.S. degree in mechanical engineering from Stanford University, Stanford, CA, in 1984.

Currently, he is an engineer with Adept Technology, Inc., San Jose, CA.